ACS OMEGA

Open Access

http://pubs.acs.org/journal/acsodf

Article

Synergistic Effect in Hybrid Plasmonic Conjugates for Photothermal Applications

Viktoriia Savchuk,* Ruizheng Wang, Lyle Small, and Anatoliy Pinchuk

Cite This: *ACS Omega* 2024, 9, 47436−47441

Read Online

ACCESS | Metrics & More | Article Recommendations | Supporting Information

ABSTRACT: Photothermal conversion efficiency (η) plays a crucial role in selecting suitable gold nanoparticles for photothermal therapeutic applications. The photothermal efficiency depends on the material used for the nanoparticles as well as their various parameters, such as size and shape. By maximizing the light-to-heat conversion efficiency (η), one can reduce the concentration of nanoparticle drugs for photothermal cancer treatment and apply lower laser power to irradiate the tumor. In our study, we explored a new hybrid plasmonic conjugate for theranostic (therapy + diagnostic) applications. We conjugated PEG-functionalized 20 nm gold nanospheres with cyanine IR dyes via a PEG linker. The resulting conjugates exhibited significantly enhanced photothermal properties compared with bare nanoparticles. We experimentally showed that a proposed new hybrid plasmonic conjugate can achieve almost four times larger conversion efficiency (47.7%) than 20 nm gold nanospheres (12%). The enhanced photothermal properties of these gold conjugates can provide the required temperature for the photothermal treatment of cancer cells with lower concentrations of gold nanoparticles injected in the body as well as with lower applied incident laser power density. Moreover, the improved photothermal properties of the conjugates can be explained by a synergistic effect that has not been observed in the past. This effect results from the coupling between the metal nanosphere and the organic dye.

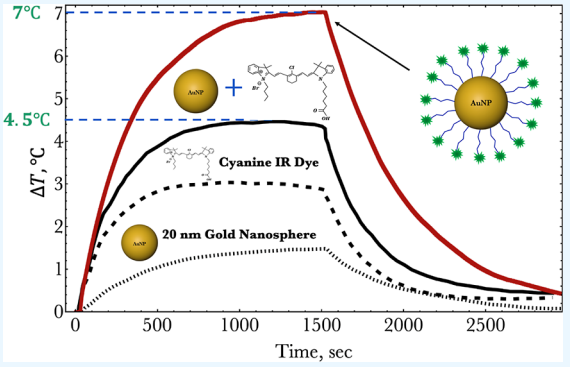

1. INTRODUCTION

Recent progress in nanotechnology has shown great promise in using plasmonic nanoparticles for Photothermal Therapy (PTT) as a noninvasive type of cancer treatment that is locally applied to the tumor.[1−4] PTT is based on the injection of metal nanoparticles directly into the tumor, followed by irradiation of the tumor with a laser. If the wavelength of the laser is matched with the localized surface plasmon resonance (LSPR) of nanoparticles, then the incident light can be effectively absorbed. Once absorbed by the nanoparticles, the light energy can be converted to thermal energy,[5−9] leading to necrosis of the targeted cancer cells.[10−14]

Gold nanoparticles are a promising candidate for PTT due to their low cytotoxicity and excellent biocompatibility.[15] Their light-to-heat photoconversion efficiency depends on the wavelengths of both LSPR and the incident light.[16]

One of the most desirable tasks of nanotechnology, including PTT for cancer treatment, is the development of multifunction drugs that can both diagnose and selectively treat only malignant cells in the body. The near-infrared (NIR) region provides the spectrum range (650−900 nm) that can be simultaneously used both in imaging and therapeutic applications, because the main components of the tissue have the lowest absorption coefficient in this range of wavelengths.[17−19] In addition, the LSPR of metal nanoparticles can be tuned to the desired wavelength in the NIR region to achieve the maximum absorption cross-section. There are several papers that have studied the photothermal properties of different shapes and sizes of gold nanoparticles, such as nanospheres, nanourchins, nanorods, nanoshells, etc., where their ability to produce sufficient heat for cancer treatment has been repeatedly demonstrated.[20−24] Different hybrid nanomaterials can also be used for PTT. For example, in refs 25−27, the authors combine and study gold-coated iron oxide nanoparticles for medical applications. Most of these studies were designed with passive accumulation in the malignant tumor site that utilizes the enhanced permeability and retention effect.[27] However, passive targeting of metal nanoparticles may and often does result in their accumulation in healthy tissues (e.g., the liver) and can lead to severe side effects. To enhance the uptake of nanoparticles by cancer cells, one can take advantage of active targeting by using gold nanoparticles conjugated with antibodies.[10,28,29] However, recent studies have shown that antibody-conjugated gold

Received: May 29, 2024
Revised: October 22, 2024
Accepted: November 13, 2024
Published: November 19, 2024

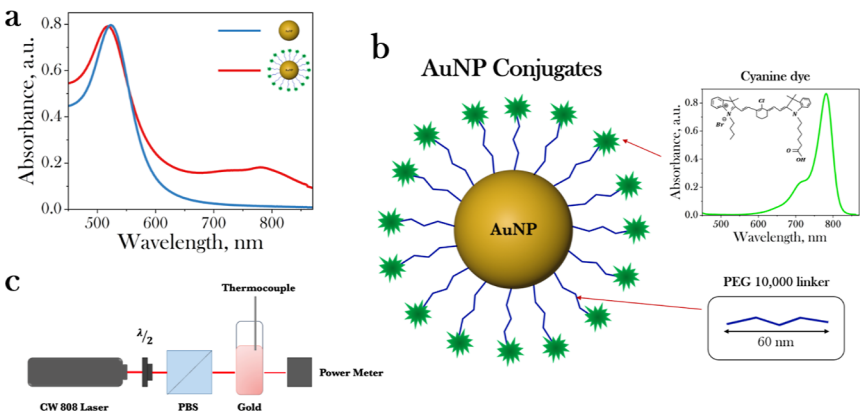

Figure 1. (a) Absorbance spectrum of 20 nm Gold Nanosphere (20 nm AuNP) and AuNPCs in UPW. (b) Schematic representation of AuNPCs with a cyanine dye absorbance spectrum. (c) Sketch of the experimental setup for measuring the temperature profiles of different solutions.

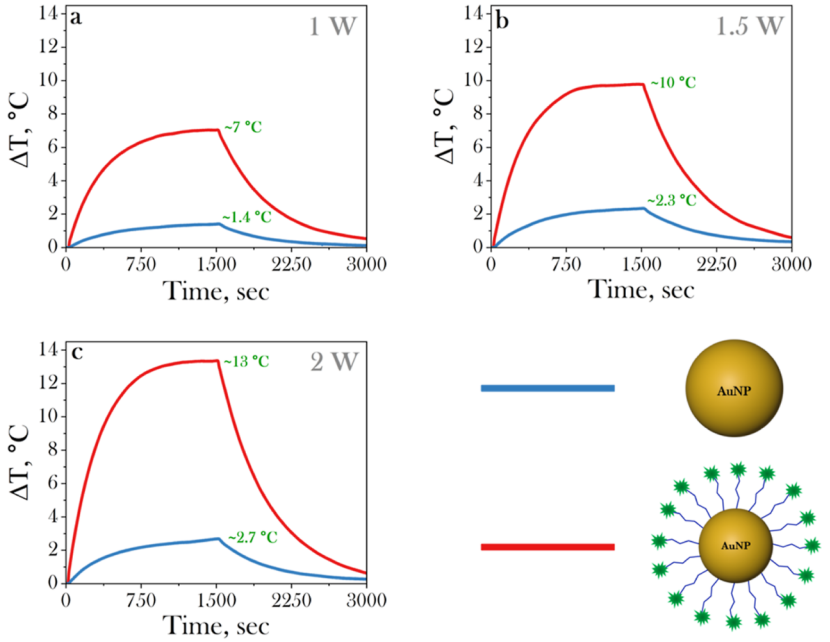

Figure 2. Temperature profiles for AuNPCs and 20 nm AuNPs in UPW for different laser powers: (a) 1 W, (b) 1.5 W, and (c) 2 W.

nanoparticles might not be the only solution for "active targeted drug delivery". Moreover, antibody-conjugated particles do not improve the photothermal properties of gold particles in general. Using infrared organic dyes as an alternative for active cancer targeting may be advantageous not only for NIR imaging of cancer,[30−33] but also it may increase the uptake of nanoparticles by the cancer cells[34−38] and potentially improve the efficacy of NIR laser treatment.

In this paper, we introduce a new hybrid plasmonic conjugated particle that can be used for theranostic (therapy + diagnostic) applications of cancer treatment. We present experimental results on the photothermal properties of spherical 20 nm gold nanoparticles (20 nm AuNPs) and 20 nm AuNPs conjugated with an organic tumor-targeting cyanine IR dye (AuNPCs) irradiated with a continuous wave (CW) of an NIR laser (λ_{in} = 808 nm). Here, we demonstrate that AuNP conjugates have LSPR in the visible spectral region around 520 nm and a second absorption peak close to the laser wavelength (λ_{in} = 808 nm) that improves their photothermal efficiency. Furthermore, we experimentally demonstrate that 20 nm AuNPs conjugated with an infrared cyanine dye exhibit a synergistic effect that leads to at least four times higher light-to-heat conversion efficiency as compared to bare 20 nm AuNPs. The enhanced photothermal properties of the AuNPCs are beneficial for their applications in PTT since they might provide the required temperature for the PTT treatment with lower concentrations of gold nanoparticles, which may also decrease the unwanted distribution of gold nanoparticles throughout the body as well as with lower incident power of the laser.

2. MATERIALS AND METHODS

The 20 nm AuNPs in ultrapurified water (UPW) (resistivity ∼18 MΩ) were purchased from Ted Pella (Redding, CA). The LSPR peak of the colloidal solution is around 520 nm (Figure 1a). The cyanine IR dyes that were used to functionalize AuNPs have an absorbance peak at the wavelength 780 nm, and they are attached to the surface of gold nanoparticles through a PEG 10,000 linker molecule of 60 nm, as shown in Figure 1b. Spherical AuNPCs in UPW were synthesized by Lahjavida (Colorado Springs, CO) by using 20 nm AuNPs purchased from Nanopartz (Loveland, CO). The colloidal

https://doi.org/10.1021/acsomega.4c05068
ACS Omega 2024, 9, 47436−47441

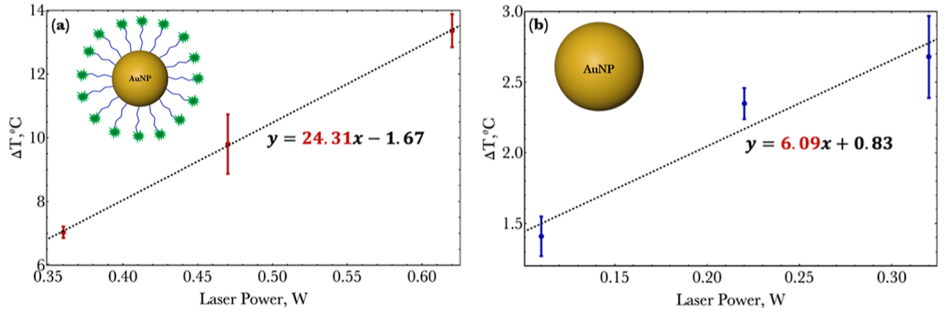

Figure 3. (a) ΔT vs $(P_0 - P_{tr})$ graph for AuNPCs. (b) ΔT vs $(P_0 - P_{tr})$ graph for 20 nm AuNPs. The error bars represent the range of the absolute value for ΔT for each solution based on measured triplicate (Figure 2).

solutions of the conjugates have two absorbance peaks around 520 and 780 nm (Figure 1a). The first peak is associated with LSPR of the gold nanosphere, and the second peak is due to the synthesis of these nanoparticles with NIR dyes. In the Supporting Information, we provide the fluorescence spectrum of cyanine IR dye solution and AuNPCs as an alternative approach to tracking the successful synthesis of dye-conjugated gold nanospheres.

Figure 1c shows the experimental setup that was used to measure the temperature profiles of the solutions under CW NIR laser irradiation. A NIR laser with a wavelength of 808 nm was used to illuminate the 20 nm AuNPs, AuNPCs, and the IR cyanine dye solutions. All solutions were prepared in a standard 4.5 mL polystyrene cuvette (Fisherbrand, Pittsburgh, PA 15275). The laser's light has elliptical polarization. A half-wave plate was used to linearly polarize the incident light, and Polarizing Beam Splitter was used to control the incident power of the laser. The temperature of the solution was recorded in real time using a temperature sensor (PS-2146, Pasco, Roseville, CA, US) connected to PASCO Capstone software. The temperature measurements were carried out in ambient room temperature (~22 °C) conditions. The transmitted power of the laser was also recorded during the experiment using a digital power meter (PM100D, Thorlabs, Dachau, Germany).

3. RESULTS AND DISCUSSION

3.1. Experimental Temperature Profiles. In this section, we present the experimental temperature profiles for 2.5 mL solutions of 20 nm AuNPs and AuNPCs in UPW. We measure temperature profiles ΔT for three different powers (here, we present the average temperature profiles for each laser's power, and we provide the experimental data for all 9 trials in the Supporting Information) of the NIR laser (λ_{in} = 808 nm). It is worth noting that the absorbance of spherical AuNPCs changes drastically after just one trial of heating (see the Supporting Information). Due to the photobleaching of dye-conjugated gold nanospheres during heating, a new solution of spherical conjugates was prepared before each trial with the concentration corresponding to Figure 1a.

The solutions of 20 nm AuNPs and AuNPCs in UPW with an absorbance ~0.79 around 520 nm were prepared for each trial (Figure 1a). By matching the LSPR peak, we assume that we have the same concentration of gold spherical nanoparticles in each solution.

Figure 2a–c shows the temperature profiles for solutions of 20 nm AuNPs and AuNPCs, AuNPs irradiated by the laser with the power P_0 = 1 W, P_0 = 1.5 W, and P_0 = 2 W, respectively. The temperature profiles were recorded for 25 min, and the same time was used to measure the cooling temperature profiles.

The maximum temperature of 13 °C was reached for AuNPCs at the power of 2 W. For 1.5 and 1 W powers, the ΔT = 10 °C and ΔT = 7 °C were recorded, respectively (Figure 2a–c). The maximum temperature for the solution of 20 nm AuNPs was 2.7 °C at a power of 2 W which is almost five times lower than the temperature increase for the same power of laser in the case of AuNP conjugates. ΔT = 1.4 °C and ΔT = 2.3 °C were reached for 20 nm AuNPs at 1.5 and 1 W powers, respectively.

AuNPCs absorb and scatter the incident light more efficiently compared to 20 nm AuNPs. This is because of the presence of the second absorbance peak near the incident wavelength of the laser (λ_2 = 780 nm) that is absent in gold nanospheres (Figure 1c).

3.2. Photothermal Conversion Efficiency. The photothermal conversion efficiency is given by (see the Supporting Information for the derivation)[39−41]

$$\eta = \frac{B(T_{max} - T_0)}{(P_0 - P_{tr})} m_W C_W \tag{1}$$

where we defined $B = \frac{hS}{m_W C_W}$ as the heat dissipation constant with m_W and C_W as mass and specific heat capacity of water, respectively. P_0 is the incident power of the laser, P_{tr} is the laser power that is transmitted through the solution, h is the heat transfer coefficient, S is the surface area of the cuvette, T_0 is the room temperature, and T_{max} is the maximum temperature the solution can reach after being irradiated by the NIR laser for 25 min.

By plotting ΔT as a function of $(P_0 - P_{tr})$, we can find the photothermal conversion efficiency for each solution.[41] The slope of Figure 3 represents the value of $\frac{\eta}{Bm_W C_W}$ expression.

The best-fit line for the ΔT vs $(P_0 - P_{tr})$ graph for AuNPCs (Figure 3a) is $y = 24.31x - 1.67$. Thus, $\frac{\eta}{Bm_W C_W} = 24.31$, and η = 47.7%. The curve-fit equation ΔT vs $(P_0 - P_{tr})$ graph for 20 nm AuNPs (Figure 3b) is $y = 6.09x + 0.83$. Therefore, $\frac{\eta}{Bm_W C_W} = 6.09$, and η = 12% (the calculations for B values are given in the Supporting Information).

The photothermal conversion efficiency of AuNPCs is almost four times larger than the photothermal conversion efficiency of bare 20 nm AuNPs. This result opens a path of using lower concentrations of drugs that potentially reduce the level of unwanted accumulation of cancer drugs in healthy tissue.

https://doi.org/10.1021/acsomega.4c05068
ACS Omega 2024, 9, 47436−47441

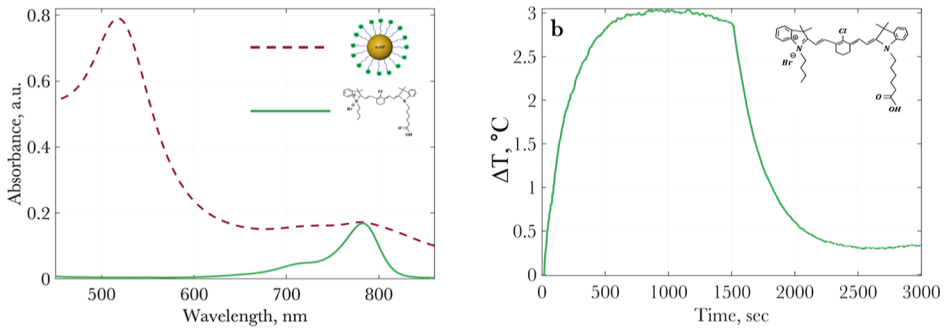

Figure 4. (a) Absorbance spectra of AuNPCs in UPW and cyanine IR dyes in methanol. (b) Temperature profile for cyanine IR dyes in methanol at laser's power of 1 W.

3.3. Synergistic Effect. We can hypothesize that a higher photothermal conversion efficiency of gold spherical conjugates results due to the additive heating produced by 20 nm AuNPs and IR cyanine dyes irradiated by the laser. In this section, we experimentally test this hypothesis by heating solutions of 20 nm AuNPs and IR cyanine dyes separately. We experimentally show that the ΔT s of each component are not additive, which leads us to discard the additive heating hypothesis. We observe a larger temperature increase for AuNPCs (gold covalently bound to the tumor-targeting dye) compared with 20 nm AuNPs and IR cyanine dye when they are added together.

Figure 4a shows the absorbance spectrum of AuNPCs in UPW and solution of IR dye in methanol (the IR cyanine dye is hydrophobic; therefore, it cannot be diluted in water). During the synthesis of AuNPCs, we cannot measure or calculate the numbers of IR cyanine dye molecules on the surface of a single gold nanosphere. AuNPCs and IR cyanine dyes represent the same absorption peaks at $\lambda_2 \sim 780$ nm. The second absorption peak of AuNPCs is due to the presence of the IR cyanine dye on the surface of the nanoparticle. Intuitively, we can assume that by matching this peak, we match the concentration of organic dyes in each solution.

Figure 4b depicts the temperature profile of IR cyanine dyes in methanol irradiated with the laser power of 1 W. The temperature increase for the solution of organic dyes is 3 °C, which is larger than ΔT for 20 nm AuNPs and less than ΔT for AuNPCs (Figure 2). The temperature profile of the solution of IR cyanine dyes resembles the temperature profile of AuNPCs. Also, during the laser's irradiation, the organic dyes reach the saturation temperature relatively quickly, and after the first 20 min, the local temperature in the solution decreases. This phenomenon is observed due to photobleaching of the dye.

By adding the temperature profile of IR cyanine dyes in methanol (Figure 4a) and the temperature profile of 20 nm AuNPs in water (Figure 2), we obtain the total temperature profile of the "mixture" solution (20 AuNPs + IR cyanine dyes) that is shown in Figure 5. The maximum temperature increase is around 4.5 °C. The temperature increase for AuNPCs, irradiated by the NIR laser light at the power of 1 W, is 7 °C (Figures 2 and 5), which is much larger than ΔT for gold nanospheres plus dye solution. Gold nanospheres conjugated with infrared dyes exhibit synergistic effects that result in higher photothermal conversion efficiency.

By conjugating gold nanospheres with IR cyanine dyes, one can induce the coupling between the metal nanoparticle and the organic emitter that leads to the dominance of the nonradiative decay rate over the radiative decay channel.[42−44]

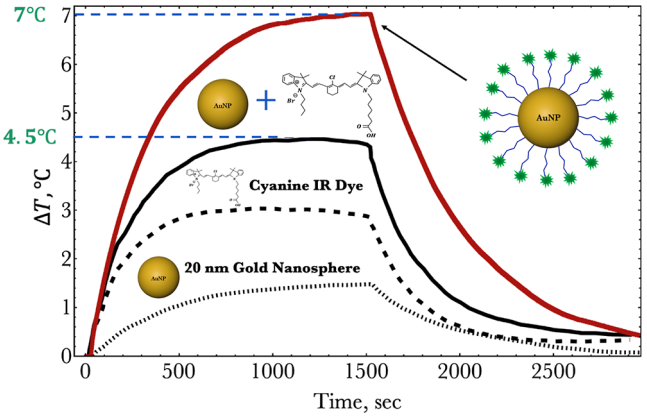

Figure 5. Temperature profile for AuNPCs in UPW, 20 nm AuNPs in UPW, IR cyanine dyes in methanol, and for 20 nm AuNPs + IR cyanine dye mixture at laser's power of 1 W.

We note that knowing the precise concentration of cyanine IR dyes in AuNPC solution can improve the study of the synergistic effect of these novel hybrid nanostructures.

4. CONCLUSIONS

Gold nanospheres conjugated with tumor-targeting organic dyes have enhanced photothermal conversion efficiency compared with bare spherical gold nanoparticles. The photothermal conversion efficiency of spherical conjugates is almost four times larger than that of gold nanospheres. We experimentally observed this strong synergistic heating effect during the laser irradiation process. We showed experimentally that by adding temperature profiles for 20 nm AuNPs and IR cyanine dyes, we do not get the same temperature increase that we observe for spherical gold conjugates. These results suggest that there is particle−dye coupling, leading to the observed synergistic effect.

Conjugated metal nanoparticles with fluorescent tumor-targeting dyes can be used as novel drugs for theranostic purposes. It is a promising platform for noninvasive imaging and treatment of a variety of cancers. In addition to the imaging modality of the dyes themselves and active targeting of the cancer tissues, the synergistic effect described above can be very beneficial for PTT. One may achieve sufficient temperatures to treat the cancer cells at a greatly reduced concentration of the drug and/or a lower power of the laser. It is expected that such structures may produce even larger photothermal properties than those discussed in this paper.

https://doi.org/10.1021/acsomega.4c05068
ACS Omega 2024, 9, 47436−47441

The photothermal properties of these novel hybrid nanostructures can be further optimized by modifying various parameters including nanoparticle morphology and linker molecule length. We expect that similar synergistic effects will be observed across different gold nanoparticle geometries. Of particular interest are the conjugates of infrared dyes with gold nanoparticles that already demonstrate high photothermal conversion efficiency within the first biological window.

■ ASSOCIATED CONTENT

Supporting Information

The Supporting Information is available free of charge at https://pubs.acs.org/doi/10.1021/acsomega.4c05068.

Fluorescence spectrum for AuNPCs and IR dyes, all three trials for experimental temperature profiles, and energy-balance equation (PDF)

■ AUTHOR INFORMATION

Corresponding Author

Viktoriia Savchuk − *Department of Physics and Energy Science, University of Colorado Colorado Springs, Colorado Springs, Colorado 80918, United States; Biofrontiers Institute and Department of Physics and Energy Science, University of Colorado Colorado Springs, Colorado Springs, Colorado 80918, United States; School of Applied and Engineering Physics, Cornell University, Ithaca, New York 14853, United States;* orcid.org/0000-0002-8964-1562; Email: vs469@cornell.edu

Authors

Ruizheng Wang − *CTI—Chromatic Technologies, Inc., Colorado Springs, Colorado 80907, United States*

Lyle Small − *CTI—Chromatic Technologies, Inc., Colorado Springs, Colorado 80907, United States*

Anatoliy Pinchuk − *Department of Physics and Energy Science, University of Colorado Colorado Springs, Colorado Springs, Colorado 80918, United States; Biofrontiers Institute and Department of Physics and Energy Science, University of Colorado Colorado Springs, Colorado Springs, Colorado 80918, United States;* orcid.org/0000-0003-1721-5668

Complete contact information is available at: https://pubs.acs.org/10.1021/acsomega.4c05068

Notes

The authors declare no competing financial interest.

■ ACKNOWLEDGMENTS

This study was supported in part by the BioFrontiers Center at the University of Colorado Colorado Springs.

■ REFERENCES

(1) Pissuwan, D.; Valenzuela, S. M.; Cortie, M. B. Therapeutic Possibilities of Plasmonically Heated Gold Nanoparticles. *Trends Biotechnol.* **2006**, *24*, 62−67.

(2) Day, E. S.; Morton, J. G.; West, J. L. Nanoparticles for Thermal Cancer Therapy. *J. Biomech. Eng.* **2009**, *131*, 074001.

(3) Hirsch, L. R.; Stafford, R. J.; Bankson, J. A.; Sershen, S. R.; Rivera, B.; Price, R. E.; Hazle, J. D.; Halas, N. J.; West, J. L. Nanoshell-Mediated Near-Infrared Thermal Therapy of Tumors Under Magnetic Resonance Guidance. *Proc. Natl. Acad. Sci. U.S.A.* **2003**, *100*, 13549−13554.

(4) Huang, X.; Jain, P. K.; El-Sayed, I. H.; El-Sayed, M. A. Plasmonic Photothermal Therapy (PPTT) Using Gold Nanoparticles. *Laser Med. Sci.* **2008**, *23*, 217−228.

(5) Baffou, G.; Quidant, R.; García de Abajo, F. J. Nanoscale Control of Optical Heating in Complex Plasmonic Systems. *ACS Nano* **2010**, *4* (2), 709−716.

(6) Baffou, G.; Quidant, R.; Girard, C. Heat Generation in Plasmonic Nanostructures: Influence of Morphology. *Appl. Phys. Lett.* **2009**, *94* (15), 153109.

(7) Jauffred, L.; Samadi, A.; Klingberg, H.; Bendix, P. M.; Oddershede, L. B. Plasmonic Heating of Nanostructures. *Chem. Rev.* **2019**, *119* (13), 8087−8130.

(8) Link, S.; El-Sayed, M. A. Shape and Size Dependence of Radiative, Non-Radiative and Photothermal Properties of Gold Nanocrystals. *Int. Rev. Phys. Chem.* **2000**, *19*, 409−453.

(9) Baffou, G.; Quidant, R. Thermo-Plasmonics: Using Metallic Nanostructures as Nano-Sources of Heat. *Laser Photonics Rev.* **2013**, *7*, 171−187.

(10) Abadeer, N. S.; Murphy, C. J. Recent Progress in Cancer Thermal Therapy Using Gold Nanoparticles. *J. Phys. Chem. C* **2016**, *120*, 4691−4716.

(11) El-Sayed, I. H.; Huang, X.; El-Sayed, M. A. Selective Laser Photo-Thermal Therapy of Epithelial Carcinoma Using anti-EGFR Antibody Conjugated Gold Nanoparticles. *Cancer Lett.* **2006**, *239*, 129−135.

(12) El-Sayed, I. H.; Huang, X.; El-Sayed, M. A. Surface Plasmon Resonance Scattering and Absorption of anti-EGFR Antibody Conjugated Gold Nanoparticles in Cancer Diagnostics; Applications in Oral Cancer. *Nano Lett.* **2005**, *5*, 829−834.

(13) Huang, X.; El-Sayed, I. H.; Qian, W.; El-Sayed, M. A. Cancer Cell Imaging and Photothermal Therapy in the Near-Infrared Region by Using Gold Nanorods. *J. Am. Chem. Soc.* **2006**, *128*, 2115−2120.

(14) Chen, C.-L.; Kuo, L.-R.; Chang, C.-L.; Hwu, Y.-K.; Huang, C.-K.; Lee, S.-Y.; Chen, K.; Lin, S.-J.; Huang, J.-D.; Chen, Y.-Y. In situ Real-Time Investigation of Cancer Cell Photothermolysis Mediated by Excited Gold Nanorod Surface Plasmons. *Biomaterials* **2010**, *31*, 4104−4112.

(15) Giljohann, D. A.; Seferos, D. S.; Daniel, W. L.; Massich, M. D.; Patel, P. C.; Mirkin, C. A. Gold Nanoparticles for Biology and Medicine. *Angew. Chem., Int. Ed.* **2010**, *49*, 3280−3294.

(16) Link, S.; El-Sayed, M. A. Size and Temperature Dependence of the Plasmon Absorption of Colloidal Gold Nanoparticles. *J. Phys. Chem. B* **1999**, *103*, 4212−4217.

(17) Weissleder, R. A clearer vision for *in vivo* imaging. *Nat. Biotechnol.* **2001**, *19*, 316−317.

(18) Frangioni, J. V. In Vivo Near-Infrared Fluorescence Imaging. *Curr. Opin. Chem. Biol.* **2003**, *7*, 626−634.

(19) Barone, P. W.; Baik, S.; Heller, D. A.; Strano, M. S. Near-Infrared Optical Sensors Based on Single-Walled Carbon Nanotubes. *Nat. Mater.* **2005**, *4*, 86−92.

(20) Moustaoui, H.; Saber, J.; Djeddi, I.; Liu, Q.; Diallo, A. T.; Spadavecchia, J.; Lamy de la Chapelle, M.; Djaker, N. Shape and Size Effect on Photothermal Heat Elevation of Gold Nanoparticles: Absorption Coefficient Experimental Measurement of Spherical and Urchin-Shaped Gold Nanoparticles. *J. Phys. Chem. C* **2019**, *123*, 17548−17554.

(21) Alrahili, M.; Peroor, R.; Savchuk, V.; McNear, K.; Pinchuk, A. Morphology Dependence in Photothermal Heating of Gold Nanomaterials with Near-Infrared Laser. *J. Phys. Chem. C* **2020**, *124* (8), 4755−4763.

(22) Cole, J. R.; Mirin, N. A.; Knight, M. W.; Goodrich, G. P.; Halas, N. J. Photothermal Efficiencies of Nanoshells and Nanorods for Clinical Therapeutic Applications. *J. Phys. Chem. C* **2009**, *113*, 12090−12094.

(23) Ma, K.; Li, Y.; Wang, Z.; Chen, Y.; Zhang, X.; Chen, C.; Yu, H.; Huang, J.; Yang, Z.; Wang, X.; Wang, Z. Core−Shell Gold Nanorod@Layered Double Hydroxide Nanomaterial with Highly Efficient Photothermal Conversion and Its Application in Antibacterial and

Tumor Therapy. *ACS Appl. Mater. Interfaces* **2019**, *11* (33), 29630−29640.
(24) Alrahili, M.; Savchuk, V.; McNear, K.; Pinchuk, A. Absorption Cross Section of Gold Nanoparticles based on NIR Laser Heating and Thermodynamic Calculations. *Sci. Rep.* **2020**, *10*, 18790.
(25) Dheyab, M. A.; Aziz, A. A.; Jameel, M. S.; Khaniabadi, P. M. Recent Advances in Synthesis, Medical Applications and Challenges for Gold-Coated Iron Oxide; Comprehensive Study. *Nanomaterials* **2021**, *11* (8), 2417.
(26) Dheyab, M. A.; Aziz, A. A.; Jameel, M. S.; Khaniabadi, P. M.; Oglat, A. A. Rapid Sonochemically-Assisted Synthesis of Highly Stable Gold Nanoparticles as Computed Tomography Contrast Agents. *Appl. Sci.* **2020**, *10* (20), 7020.
(27) Maeda, H.; Greish, K.; Fang, J. The EPR Effect and Polymeric Drugs: A Paradigm Shift for Cancer Chemotherapy in the 21st Century. *Adv. Polym. Sci.* **2005**, *193* (1), 103−121.
(28) Green, H. N.; Martyshkin, D. V.; Rodenburg, C. M.; Rosenthal, E. L.; Mirov, S. B. Gold Nanorod Bioconjugates for Active Tumor Targeting and Photothermal Therapy. *J. Nanotechnol.* **2011**, *2011*, 631753.
(29) Liao, H.; Hafner, J. H. Gold Nanorod Bioconjugates. *Chem. Mater.* **2005**, *17* (18), 4636−4641.
(30) Tsujino, Y.; Mizumoto, K.; Matsuzaka, Y.; Niihara, H.; Morita, E. Fluorescence Navigation with Indocyanine Green for Detecting Sentinel Nodes in Extramammary Paget's Disease and Squamous Cell Carcinoma. *J. Dermatol.* **2009**, *36*, 90−94.
(31) Li, T.; Li, C.; Ruan, Z.; Xu, P.; Yang, X.; Yuan, P.; Wang, Q.; Yan, L. Polypeptide-Conjugated Second Near-Infrared Organic Fluorophore for Image-Guided Photothermal Therapy. *ACS Nano* **2019**, *13*, 3691−3702.
(32) Jiang, X.; Du, B.; Huang, Y.; Yu, M.; Zheng, J. Cancer Photothermal Therapy with ICG-Conjugated Gold Nanoclusters. *Bioconjugate Chem.* **2020**, *31* (5), 1522−1528.
(33) Rosenthal, E. L.; Warram, J. M.; Boer, E.; Chung, T. K.; Korb, M. L.; Brandwein-Gensler, M.; Strong, T. V.; Schmalbach, C. E.; Morlandt, A. B.; Agarwal, G.; Hartman, Y. E.; Carroll, W. R.; Richman, J. S.; Clemons, L. K.; Nabell, L. M.; Zinn, K. R. Safety and Tumor Specificity of Cetuximab-IRDye800 for Surgical Navigation in Head and Neck Cancer. *Clin. Cancer Res.* **2015**, *21* (16), 3658−3666.
(34) Shi, C.; Wu, J. B.; Chu, G. C.-Y.; Li, Q.; Wang, R.; Zhang, C.; Zhang, Y.; Kim, H. L.; Wang, J.; Zhau, H. E.; Pan, D.; Chung, L. W. K. Heptamethine Carbocyanine Dye-Mediated Near-Infrared Imaging of Canine and Human Cancers through the HIF-1α/OATPs signaling axis. *Oncotarget* **2014**, *5*, 10114−10126.
(35) Choi, P. J.; Park, T. I.-H.; Cooper, E.; Dragunow, M.; Denny, W. A.; Jose, J. Heptamethine Cyanine Dye Mediated Drug Delivery: Hype or Hope. *Bioconjugate Chem.* **2020**, *31*, 1724−1739.
(36) Marker, S. C.; Espinoza, A. F.; King, A. P.; Woodfield, S. E.; Patel, R. H.; Baidoo, K.; Nix, M. N.; Ciaramicoli, L. M.; Chang, Y.; Escorcia, F. E.; Vasudevan, S. A.; Schnermann, M. J. development of Iodinated Indocyanine Green Analogs as a Strategy for Targeted Therapy of Liver Cancer. *ACS Med. Chem. Lett.* **2023**, *14* (9), 1208−1215.
(37) Park, M. H.; Jo, G.; Lee, B. Y.; Kim, E. J.; Hyun, H. Rapid Tumor Targeting of Renal-clearable ZW800−1 Conjugate for Efficient Photothermal Cancer Therapy. *Biomedicines* **2021**, *9* (9), 1151.
(38) Sharma, A.; Verwilst, P.; Li, M.; Ma, D.; Singh, N.; Yoo, J.; Kim, Y.; Yang, Y.; Zhu, J.; Huang, H.; Hu, X.; He, X.; Zeng, L.; James, T. D.; Peng, X.; Sessler, J. L.; Kim, J. S. Theranostic Fluorescent Probes. *Chem. Rev.* **2024**, *124* (5), 2699−2804.
(39) Roper, D. K.; Ahn, W.; Hoepfner, M. Microscale Heat Transfer Transduced by Surface Plasmon Resonant Gold Nanoparticles. *J. Phys. Chem. C* **2007**, *111*, 3636−3641.
(40) Richardson, H. H.; Carlson, M. T.; Tandler, P. J.; Hernandez, P.; Govorov, A. O. Experimental and Theoretical Studies of Light-to-Heat Conversion and Collective Heating Effects in Metal Nanoparticle Solutions. *Nano Lett.* **2009**, *9*, 1139−1146.
(41) Jiang, K.; Smith, D. A.; Pinchuk, A. Size-Dependent Photothermal Conversion Efficiencies of Plasmonically Heated Gold Nanoparticles. *J. Phys. Chem. C* **2013**, *117*, 27073−27080.
(42) Dulkeith, E.; Morteani, A. C.; Niedereichholz, T.; Klar, T. A.; Feldmann, J.; Levi, S. A.; van Veggel, F. C. J. M.; Reinhoudt, D. N.; Möller, M.; Gittins, D. I. Fluorescence Quenching of Dye Molecules near Gold Nanoparticles: Radiative and Nonradiative Effects. *Phys. Rev. Lett.* **2002**, *89*, 203002.
(43) Savchuk, V.; Knize, A. R.; Pinchuk, P.; Pinchuk, A. O. Size-Dependent Emission of a Dipole Coupled to a Metal Nanoparticle. *MRS Adv.* **2020**, *5* (62), 3315−3325.
(44) Savchuk, V. V.; Gamernyk, R. V.; Virt, I. S.; Malynych, S. Z.; Pinchuk, A. O. Plasmon-Exciton Coupling in Nanostructured Metal-Semiconductor Composite Films. *AIP Adv.* **2019**, *9*, 045021.

https://doi.org/10.1021/acsomega.4c05068
ACS Omega 2024, 9, 47436−47441